Supporting Information

Becattini et al. 10.1073/pnas.1106698108

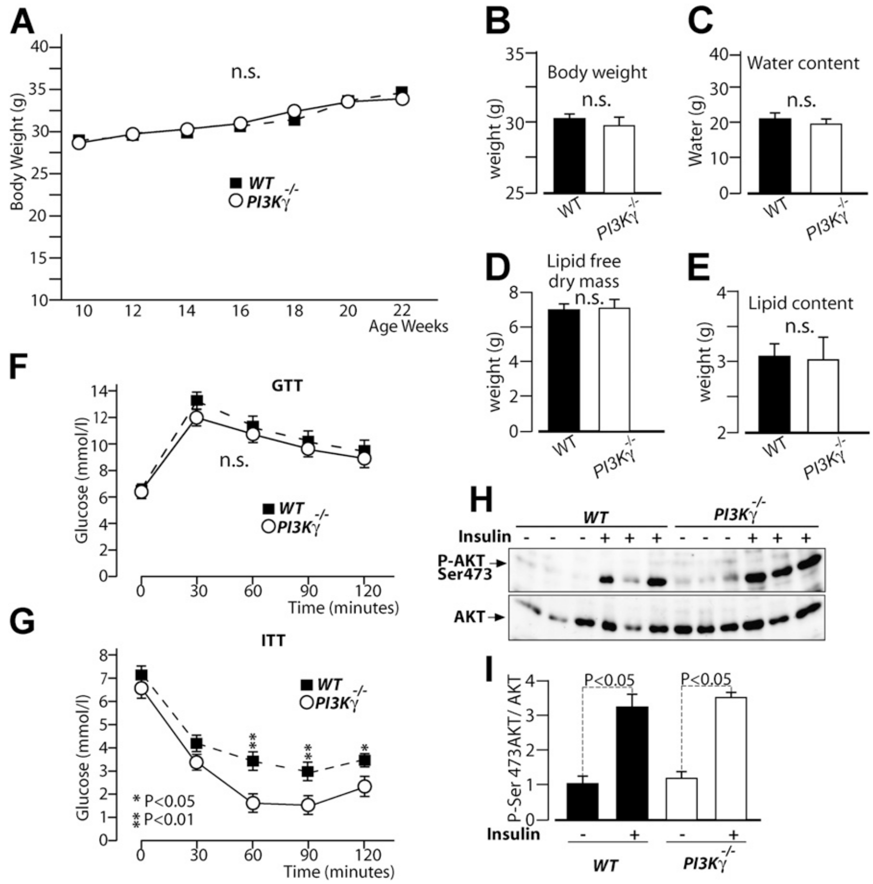

Fig. S1. PI3K$\gamma^{-/-}$ mice placed on chow diet display comparable growth curves with WT mice and marginally improved glucose homeostasis. (*A*) Growth curves of WT and *PI3K*$\gamma^{-/-}$ mice placed on chow diet. (*B–E*) Body composition of WT and *PI3K*$\gamma^{-/-}$ mice placed on chow diet. (*F*) Glucose tolerance test (GTT) and (*G*) insulin tolerance test (ITT) of WT and *PI3K*$\gamma^{-/-}$ mice placed on chow diet at the age of 20 wk. (*H* and *I*) Immunoblot analysis of protein kinase B (PKB)/AKT phosphorylation in extensor digitorum longus muscles stimulated ex vivo with 0.1 μM insulin. Data are represented as mean, and error bars indicate SEM.

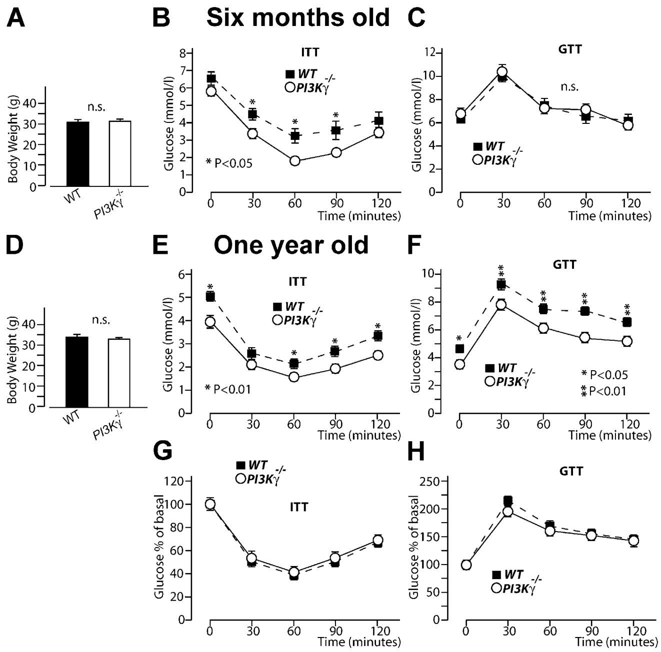

Fig. S2. *PI3Kγ*$^{-/-}$ mice are protected from aging-induced glucose intolerance. (*A*) Body weight, (*B*) ITT, and (*C*) GTT of WT and *PI3Kγ*$^{-/-}$ mice placed on chow diet at the age of 6 mo. (*D*) Body weight, (*E*) ITT, and (*F*) GTT of WT and *PI3Kγ*$^{-/-}$ mice placed on chow diet at the age of 1 y. (*G* and *H*) The GTT and ITT data from *E* and *F* are here presented as percent variation from baseline. Data are represented as mean, and error bars indicate SEM.

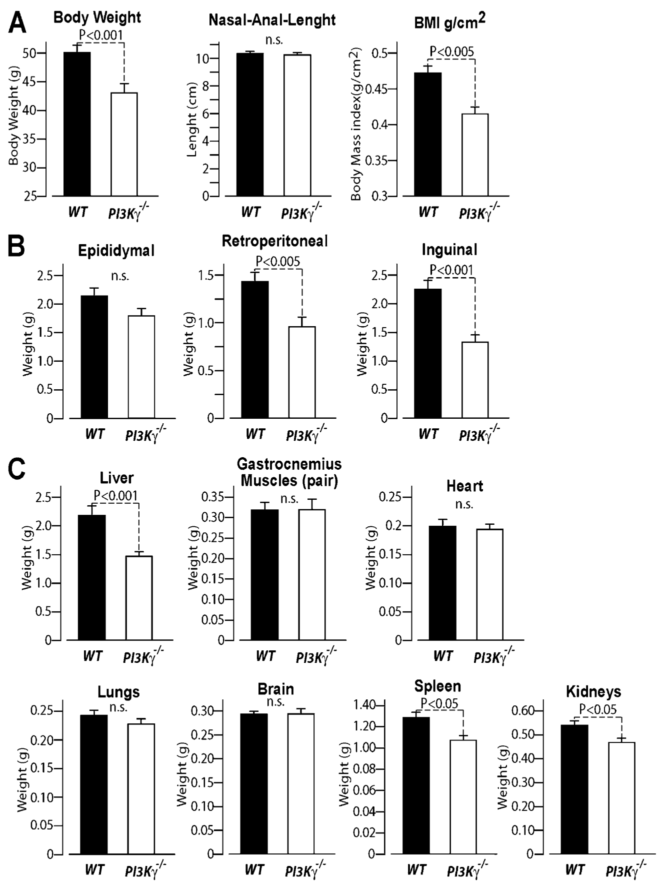

Fig. S3. *PI3Kγ*$^{-/-}$ mice placed on high-fat obesogenic diet (HFD) display reduced body mass index and adiposity. (*A*) Body weight, nasal–anal length, and body mass index of WT and *PI3Kγ*$^{-/-}$ mice placed on HFD at the age of 8 wk for 12 wk. (*B*) Weight of different fat pads from the mice above. (*C*) Weight of different tissues from the mice above. Data are represented as mean, and error bars indicate SEM.

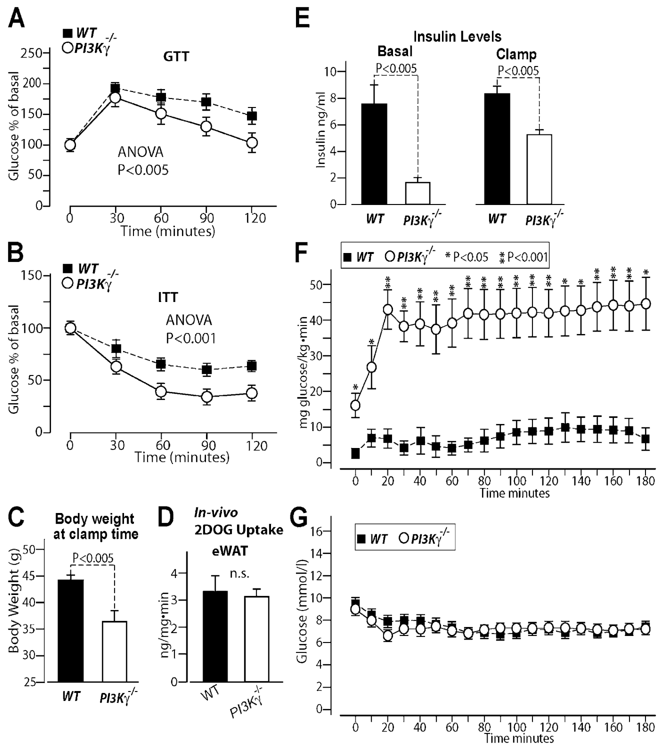

Fig. S4. $PI3K\gamma^{-/-}$ mice placed on HFD display improved insulin sensitivity compared with WT mice. (*A* and *B*) The GTT and ITT data from Fig. 2 *A* and *B* are here presented as percent variation from baseline. (*C*) Body weight of WT and $PI3K\gamma^{-/-}$ mice on the day of the clamp described in Fig. 2. (*D*) 2-Deoxy-D-glucose (2DOG) uptake in epididymal white adipose tissue during the clamp. (*E*) Plasma insulin levels before clamp (basal) and during steady glucose and insulin infusion (clamp). (*F*) Glucose infusion rates and (*G*) blood glucose levels during the hyperinsulinemic euglycemic clamp.

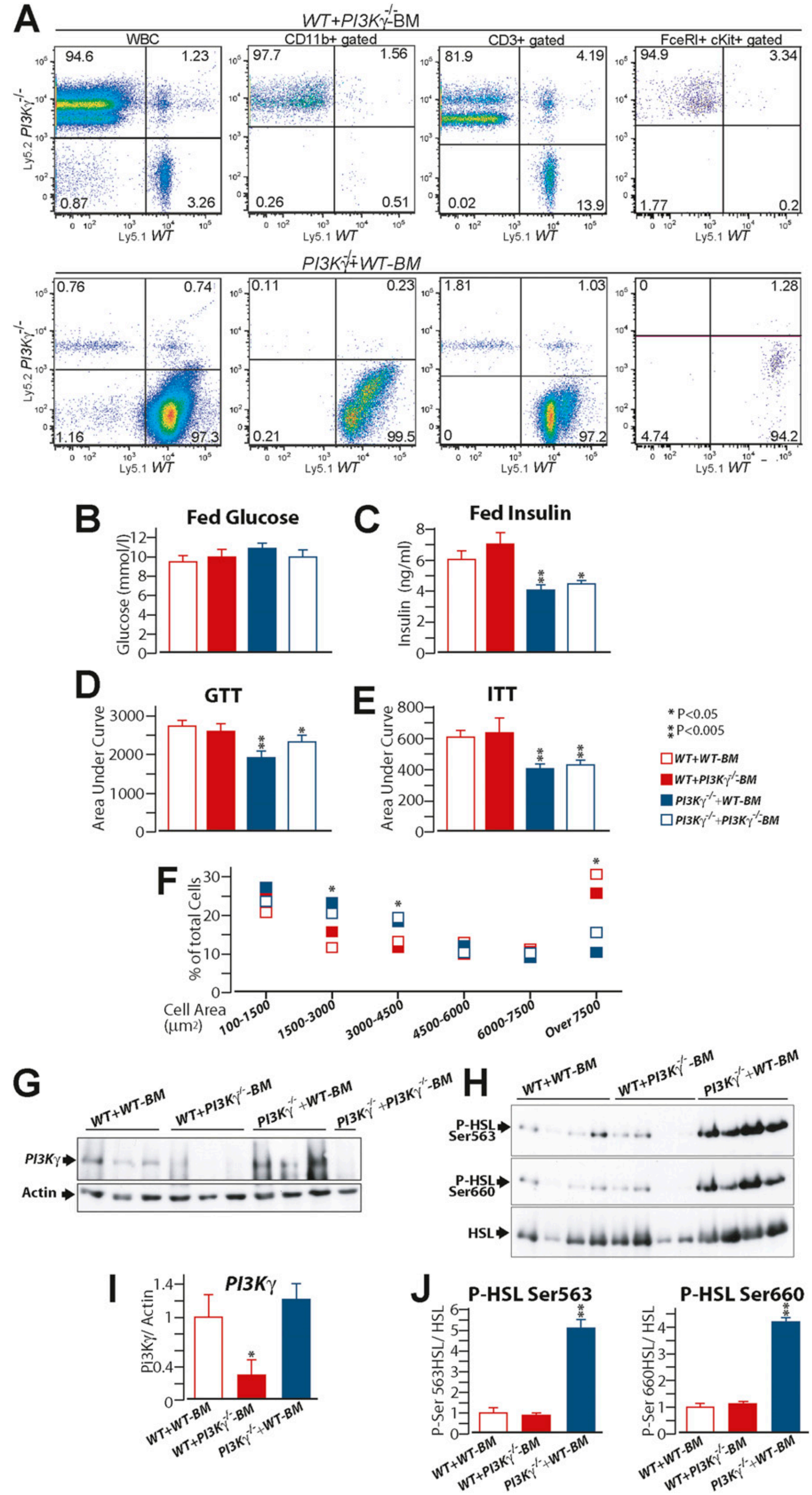

Fig. S5. Bone marrow transplantation study. (*A*) Flow cytometry analysis of reconstitution of the radiation chimeras in Fig. 3: total white blood cells (WBC), CD11b$^+$ blood cells (peripheral blood monocytes), CD3$^+$ blood cells (lymphocytes), and FcεRI$^+$ cKit$^+$ peritoneal cells (mast cells). *PI3Kγ*$^{-/-}$ cells express the Ly5.2 marker, whereas WT cells express the Ly5.1 marker. (*B*) Blood-fed glucose levels and (*C*) fed insulin levels of the different radiation chimeras. (*D* and *E*) Area under the curve of the GTTs and ITTs described in Fig. 3. (*F*) Adipocyte size distribution measured from the white adipose tissue sections described in Fig. 3 *F* and *G*. The asterisks indicate $P < 0.05$ for either *PI3Kγ*$^{-/-}$ + *WT-BM* or *PI3Kγ*$^{-/-}$ + *PI3Kγ*$^{-/-}$*-BM* vs. controls *WT* + *WT-BM*. (*G*) Immunoblot analysis of PI3Kγ protein levels in white adipose tissues from the radiation chimeras described in Fig. 3. (*H*) Immunoblot analysis of protein kinase A (PKA)-dependent hormone-sensitive lipase phosphorylation in white adipose tissues from the radiation chimeras described in Fig. 3. (*I* and *J*) Quantification of the immunoblots in *G* and *H*. Data are represented as mean ± SEM.

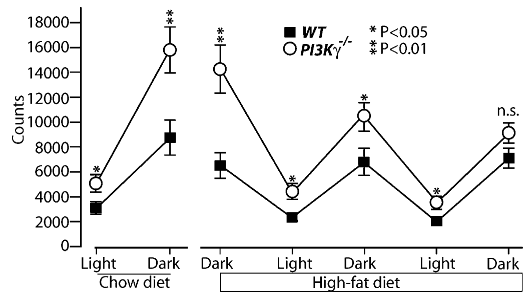

Fig. S6. *PI3Kγ*$^{-/-}$ mice display increased physical activity relative to WT control mice. Physical activity was evaluated in *PI3Kγ*$^{-/-}$ and WT mice by infrared beams breaking during the calorimetry described in Fig. 4 *I* and *J*. Data are represented as mean ± SEM.

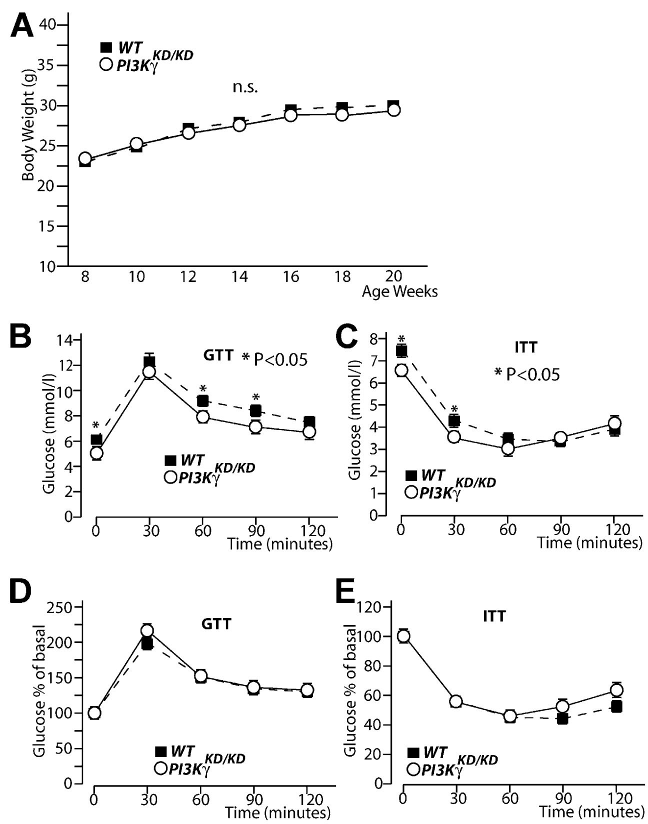

Fig. S7. *PI3Kγ*$^{KD/KD}$ mice placed on chow diet display comparable growth curves to WT control mice and marginally improved glucose homeostasis. (*A*) Growth curves of WT and *PI3Kγ*$^{KD/KD}$ mice placed on chow diet. (*B*) GTT and (*C*) ITT of WT and *PI3Kγ*$^{KD/KD}$ mice placed on chow diet at the age of 20 wk. (*D* and *E*) The GTT and ITT data from *B* and *C* are here presented as percent variation from baseline. Data are represented as mean, and error bars indicate SEM.

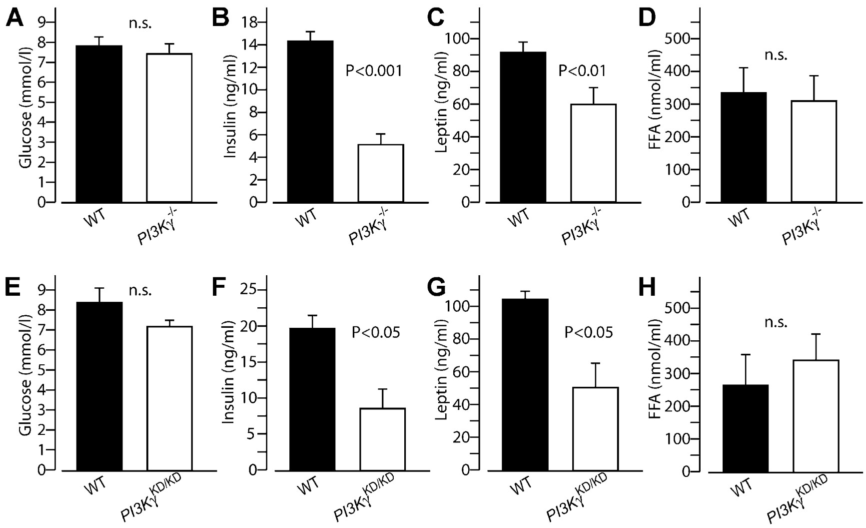

Fig. S8. *PI3K*$\gamma^{-/-}$ and *PI3K*$\gamma^{KD/KD}$ mice display decreased plasma leptin but similar free fatty acids (FFA) compared with WT mice. (*A*) Fed plasma glucose, (*B*) plasma insulin (*C*) leptin, and (*D*) FFA levels from the mice described in Fig. 2. (*E*) Fed plasma glucose, (*F*) plasma insulin, (*G*) leptin, and (*H*) FFA levels from the mice described in Fig. 6. Data are represented as mean ± SEM.

Table S1. List of primers used for quantitative PCR

Target sequence	Forward	Reverse
IL-1β	GCAACTGTTCCTGAACTCAACT	TCTTTTGGGGTCCGTCAACT
F4/80	CTTTGGCTATGGGCTTCCAGTC	GCAAGGAGGACAGAGTTTATCGTG
FceRI	TAGCACTGCTGTTCATGTCTC	GAGTTCATTTGAAGGTGATTGTT
TNF-α	CCCCAAAGGGATGAGAAGTT	CTCCTCCACTTGGTGGTTTG
MCP-1	CCCCAAGAAGGAATGGGTCC	GGTTGTGGAAAAGGTAGTGG
MIP-1 (ccl3)	TTCTCTGTACCATGACACTCTGC	CGTGGAATCTTCCGGCTGTAG
Osteopontin (spp1)	TCCCTCGATGTCATCCCTGT	CCCTTTCCGTTGTTGTCCTG
PAI (serpine1)	TCCTCATCCTGCCTAAGTTCTC	GTGCCGCTCTCGTTTACCTC
CXCL14	TAGCTGGAGCGAGCCGAGCA	GGGGAGCAGGGAGGCAAGGA
IL1-Ra	AAATCTGCTGGGGACCCTAC	TCTTCTAGTTTGATATTTGGTCCTTG
IL-6	TCCTACCCCAATTTCTGCTC	TTGGATGGTCTTCCTTAGCC
Cyclophilin	ATGGTCAACCCCACCGTGT	TTTCTGCTGTCTTTGGAACTTTGTC